Stabilization of Inorganic Perovskite Solar Cells with a 2D Dion–Jacobson Passivating Layer

Luyan Wu, Guixiang Li,* Karunanantharajah Prashanthan, Artem Musiienko, Jinzhao Li, Thomas W. Gries, Hao Zhang, Hans Köbler, Patryk Janasik, Augustine N. S. Appiah, Gopinath Paramasivam, Tianxiao Sun, Meng Li, Daniela Marongiu, Michele Saba,* and Antonio Abate*

Inorganic metal halide perovskites such as $CsPbI_3$ are promising for high-performance, reproducible, and robust solar cells. However, inorganic perovskites are sensitive to humidity, which causes the transformation from the black phase to the yellow δ, non-perovskite phase. Such phase instability has been a significant challenge to long-term operational stability. Here, a surface dimensionality reduction strategy is reported, using 2-(4-aminophenyl)ethylamine cation to construct a Dion–Jacobson 2D phase that covers the surface of the 3D inorganic perovskite structure. The Dion–Jacobson layer mainly grows at the grain boundaries of the perovskite, effectively passivating surface defects and providing favourable interfacial charge transfer. The resulting inorganic perovskite films exhibit excellent humidity resistance when submerged in an aqueous solution (isopropanol:water = 4:1 v/v) and exposed to a 50% humidity air atmosphere. The Dion–Jacobson 2D/3D inorganic perovskite solar cell (PSC) achieves a power conversion efficiency (PCE) of 19.5% with a V_{oc} of 1.197 eV. It retains 83% of its initial PCE after 1260 h of maximum power point tracking under 1.2 sun illumination. The work demonstrates an effective way for stabilizing efficient inorganic perovskite solar cells.

1. Introduction

Inorganic metal halide perovskites have been drawing significant attention due to their remarkable thermal stability (absence of volatile constituents),[1,2] good photostability (lack of phase segregation),[3] and suitable bandgap (1.7 eV) for photovoltaics.[4,5] Solar cells based on inorganic perovskites have shown improved power conversion efficiency (PCE), from 2.9%[6] in 2015 to 21.3%[7] at present.

However, inorganic perovskites are extremely sensitive to humidity, which triggers the transformation from the photoactive black phase to the δ yellow, non-perovskite phase.[8,9] Such degradation seriously challenges the stability of inorganic solar cells and represents the most severe impediment to their commercialization potential. Several strategies have been proposed to improve perovskite intrinsic humidity stability, e.g., the use of

L. Wu, D. Marongiu, M. Saba
Dipartimento di Fisica
Università degli Studi di Cagliari
Monserrato (CA) I-09042, Italy
E-mail: saba@unica.it

L. Wu, G. Li, K. Prashanthan, A. Musiienko, J. Li, T. W. Gries, H. Köbler, G. Paramasivam, T. Sun, A. Abate
Helmholtz-Zentrum Berlin für Materialien und Energie GmbH
Hahn-Meitner-Platz 1, 14109 Berlin, Germany
E-mail: guixiang.li@epfl.ch; antonio.abate@helmholtz-berlin.de

G. Li
Institute of Chemical Sciences and Engineering
École Polytechnique Fédérale de Lausanne (EPFL)
Lausanne 1015, Switzerland

G. Li, A. Abate
Department of Chemistry
Bielefeld University
Universitätsstraße 25, 33615 Bielefeld, Germany

K. Prashanthan
Department of Physics
University of Jaffna
Jaffna 40000, Sri Lanka

H. Zhang
Laboratoire Ondes et Matière d'Aquitaine
Université de Bordeaux & CNRS
Talence 33405, France

P. Janasik, A. N. S. Appiah
Department of Chemistry
Silesian University of Technology
Strzody 9, Gliwice 44–100, Poland

**ADVANCED
SCIENCE NEWS**

www.advancedsciencenews.com

**ADVANCED
MATERIALS**

www.advmat.de

2D perovskites, ionic incorporation,[10] regulating surface energy[11] as well as surface termination.[12] Among these efforts, introducing a 2D perovskite capping layer on top of 3D perovskites is an effective way to realize a hydrophobic surface within the solar cell and prevent humidity from reacting with the inorganic perovskite. Compared with 3D perovskites, 2D perovskites consist of layered perovskites and organic cations sheets, a structure that confers outstanding humidity stability and tuneable bandgap. However, since the aligned organic cation spacer usually acts as an insulating layer between conducting layers of inorganic metal halide octahedra, it significantly hinders charge transport. Consequently, employing thick layers of 2D perovskites makes optimization of efficiency and stability of solar cells often incompatible.[13,14] Construction of 2D/3D stacking structures with a thin 2D layer can combine the advantages of enhanced stability in 2D perovskites with strong light absorption and good charge carrier-transport properties in 3D perovskite materials. Therefore, the 2D/3D heterostructure is considered a crucial element in preserving the high efficiency of PSCs while improving device stability.[15] Phenethyl ammonium iodide (PEAI) to form $PEA_2PbI_4/CsPbI_3$,[16] and phenyl trimethylammonium iodide (PTAI) to construct a $PTA_2PbI_4/CsPbI_3$ heterostructure have been demonstrated to improve both efficiency and stability.[17] Such heterostructures have involved Ruddlesden–Popper (RP) 2D perovskite, where successive metal halide octahedra layers have staggered arrangements, and van der Waals forces between adjacent cations' sheets significantly distort the 2D perovskite structure. The Dion–Jacobson type of 2D perovskites,[16,18–20] where the metal halide slabs are all aligned, have been much less explored, even though their structure should be more stable than their RP counterparts and van der Waals forces do not play a significant role.[21] To our knowledge, this is the first time to report depositing a 2D Dion–Jacobson layer on all inorganic $CsPbI_3$ solar cells to improve its stability.

In this work, we set out to investigate the potential of Dion–Jacobson 2D perovskites to improve the stability of photovoltaic devices based on inorganic perovskites. 2-(4-Aminophenyl)ethylamine (PMEA) cation was used to form a layer of 2D Dion–Jacobson perovskite and modify the surface of the 3D $CsPbI_3$ perovskite film. After the 2D perovskite was formed, 2D/3D perovskite solar cells (PSCs) achieved a PCE of 19.5% with an open circuit voltage (V_{oc}) of 1.197 V. The improved PCEs are attributed to decreased trap concentration facilitating recombination at the interface. Additionally, the treatment with the 2D layer improved the stability of the 3D film, with the black phase preserved four times longer than in the pure 3D film when immersed in an aqueous solution of isopropanol (IPA:water =

4:1 v/v). Upon exposure to 47%−56% humidity at room temperature, the pure 3D perovskite started to degrade after 0.5 hours, but the 2D/3D perovskite still maintained a pure phase after 3.5 h. The PMEA-based devices retained 83% of their PCE after 1260 h of MPP tracking under 1.2 sun illumination and showed excellent stability against exposure to humidity and heat (85 °C) in the air atmosphere.

2. Results and Discussion

The schematic illustration of the 2D/3D multilayer structure is shown in **Figure 1**A, where the 3D perovskite is $CsPbI_3$, and the 2D one is $PMEA_2PbI_4$. The sketch of the organic cation [2-(4-aminophenyl)ethyl]ammonium diiodine ($PMEAI_2$) is shown in Figure 1B. The diammonium diiodide was synesized by a reaction between [2-(4-aminophenyl)ethyl]ammonium and HI acid. In this work, we used isopropanol (IPA) to dissolve $PMEAI_2$, then spin-coated its solution on the top to 3D perovskites. We conducted grazing-incidence X-ray diffraction (GIXRD) to verify the formation of the 2D layer. As displayed in Figure 1B, after annealing and depositing $PMEAI_2$ solution on the surface of $CsPbI_3$ perovskite, we observed the signature of the formation of the 2D phase in the form of an additional diffraction peak at low angles (5.7°). Grazing-incidence wide-angle X-ray scattering (GIWAXS) was further measured (see Figure 1C,D). The reference film only displayed diffraction features corresponding to the $CsPbI_3$ phase, where $q_r = 1.0, 1.4$ Å refer to the (110) and (020) planes, respectively. Besides these diffraction rings of pure 3D, an additional diffraction arch was visible in the 2D/3D film at $q_r = 0.4$, which was attributed to the (001) planes of the 2D phase. Furthermore, the (110)/(020) peak intensity ratio increased from 2.36 to 2.69 after 2D passivation, indicating that the presence of a 2D perovskite layer has induced the preferential orientation of the (110) crystallographic planes on the surface(Figure S2, Supporting Information). The shift of N–H vibration peaks, shown in Fourier transform infrared (FTIR) spectra (Figure S3, Supporting Information), verified the interaction between PMEA cation and perovskite. Figure S4 (Supporting Information) shows the top view morphologies of reference and 2D/3D perovskite films utilized by scanning electron microscopy (SEM). Many pinholes were observed in the reference film in Figure S4A,C (Supporting Information), while pinholes were not detected at the surface of 2D/3D film (Figure S4B,D, Supporting Information). Cross-sectional SEM images in Figure S4E,F (Supporting Information) shows that the thickness of reference and 2D/3D films were 406 and 411 nm, respectively.

Since the black phase in $CsPbI_3$ films transforms into the δ phase quickly when exposed to a humid environment, improving moisture tolerance is critical for the stability of $CsPbI_3$ solar cells. We systematically investigated the effect of the 2D surface layer on stability against humidity. We started with water contact angle measurements to evaluate the influence of a thin layer of 2D on the surface wettability. As shown in **Figure 2**A, after depositing a layer of 2D perovskite, the water contact angle of the treated film was 52°, higher than the 34° value for the reference film and providing a first hint that moisture resistance was improved. We immersed perovskite films in a mixture of solvents (water:IPA = 1:4 v/v) to examine the time-dissolved film moisture stability. The process is displayed in Video S1 (Supporting

M. Li
Key Lab for Special Functional Materials of Ministry of Education
National & Local Joint Engineering Research Center for High-efficiency
Display and Lighting Technology
School of Materials Science and Engineering
Collaborative Innovation Center of Nano Functional Materials and
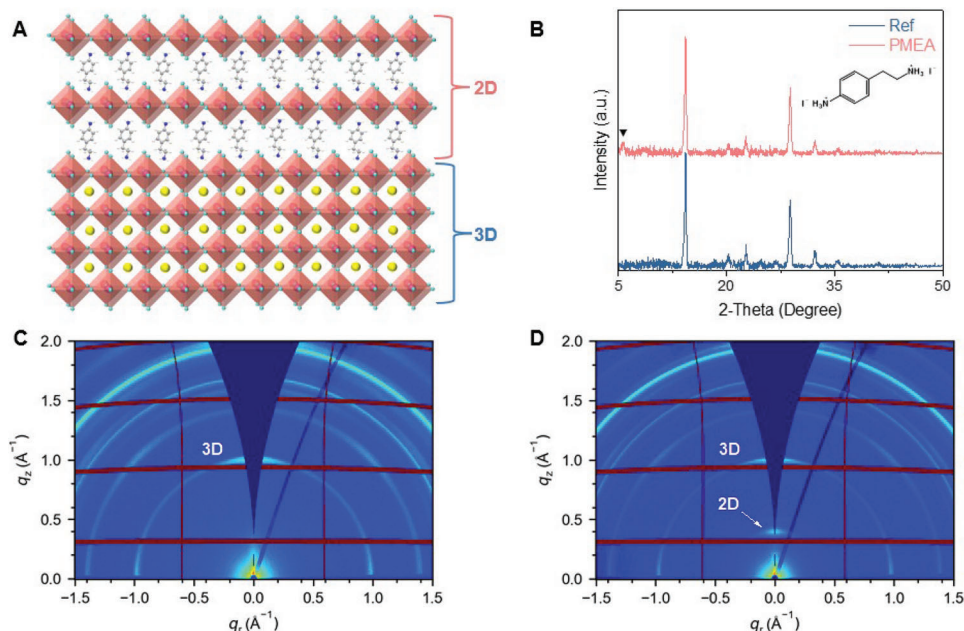Applications
Henan University
Kaifeng 475004, P. R. China

Figure 1. Surface dimensionality reduction for inorganic perovskites. A) Schematic illustration of the 2D/3D perovskite interface. B) XRD patterns at 0.5 incident angle of 2D/3D and reference film, where "▼" indicates the 2D perovskite phase, and the inserted molecular structure is PMEA cation. C,D) are grazing-incidence wide-angle X-ray scattering (GIWAXS) data of pure 3D and 2D/3D perovskite films (angle of incidence = 0.15°).
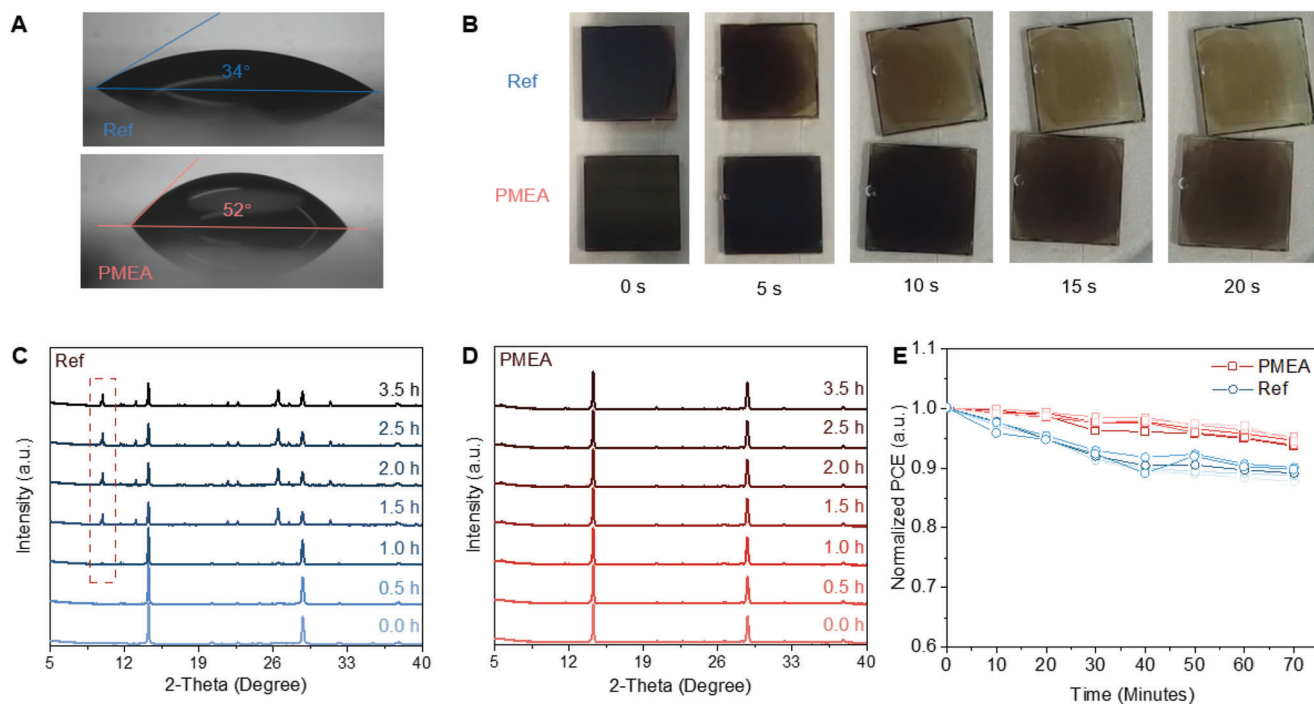

Figure 2. 2D/3D structure enhanced film humidity stability. A) Water contact angle measurement for reference (top) and 2D/3D (bottom) perovskite films. B) Optical images of reference (top) and 2D/3D (bottom) films exposed to a mixture solvent (water:IPA = 1:4 v/v) at different times (simultaneously present in the same solution). C,D) XRD patterns of reference and 2D/3D films exposure to 47%−56% humidity air atmosphere at different times, the zoom graph for the selected area is in Figure S6 (Supporting Information). E) Time-dependence PCE profiles of reference and 2D/3D perovskite devices under air atmosphere with 20% humidity.
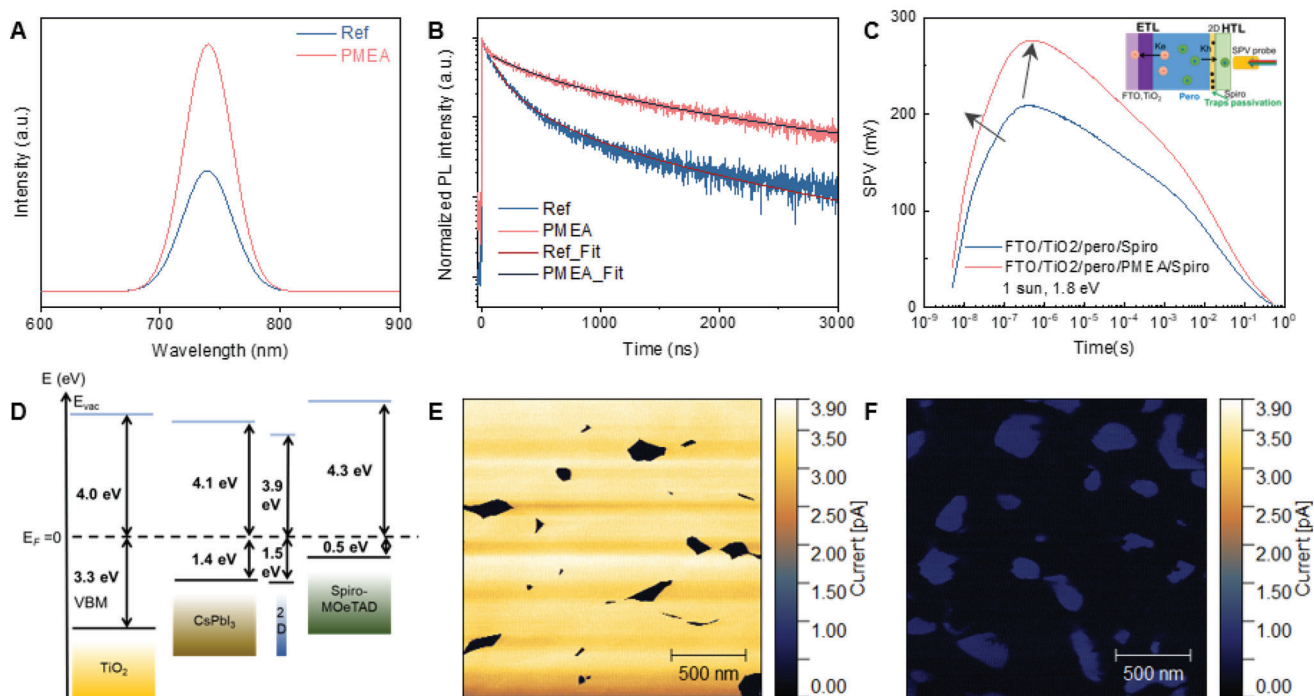
**ADVANCED
SCIENCE NEWS**

www.advancedsciencenews.com

**ADVANCED
MATERIALS**

www.advmat.de

Figure 3. Improved charge-transport properties. A) Steady-state PL spectra and B) time-dependent PL of the films without and with 2D passivation. C) SPV transient spectra of FTO/TiO$_2$/perovskite/Spiro film with and without a 2D interlayer. The excitation wavelength is 689 nm, above the bandgap of inorganic perovskite (1.7 eV). The inset demonstrates charge extraction, which induces a trSPV signal. D) Schematic diagram of energy level arrangement of prepared PSCs with or without 2D interlayer. E,F) are CAFM images of reference and 2D/3D perovskite films.

Information). The pictures extracted from Video S1 (Supporting Information) show that the reference film turned yellow after 5 s, while the 2D/3D film remained in the black phase significantly longer (Figure 2B). We measured XRD as a function of exposure time to analyse structural modifications after film exposure to air atmosphere with 47%–56% humidity. The results are displayed in Figure 2C,D. The peaks at 10°, 13°, and 26°, related to the yellow δ phase, started to appear after 0.5 h for the reference film. In contrast, only the pure black phase without δ phase peak was detected after 3.5 h in the 2D/3D perovskite film, demonstrating the protective effect provided to CsPbI$_3$ by the deposition of the 2D perovskite layer.

We proceeded to study the effect of the 2D layer on the stability and efficiency of solar cells by fabricating both reference and 2D/3D perovskite devices and testing them in the air. 2D/3D devices maintained 95% of their original efficiency after 70 min in an ambient atmosphere, while the performance of pure 3D perovskites degraded faster (Figure 2E). To study the effect of the 2D layer in high-temperature conditions, we placed the devices on an 85 °C hot plate in an air atmosphere (20% humidity) and measured photoluminescence (PL) spectra as a function of time. Figure S5 (Supporting Information) shows that in reference devices, luminescence disappeared after 6 h, while with the 2D layer, intense luminescence was measured even after the reference sample was degraded.

We conducted several charge-transport characterization measurements to study the effect of the 2D passivation layer on charge transport. First, we compared steady-state and time-resolved PL (TRPL) measurements for reference and 2D/3D per-

ovskite films to investigate the charge carrier recombination dynamics. The steady-state PL emission intensity of the 2D/3D heterostructure film was two times more intense than the one from the reference film (**Figure 3**A), hinting at a significant suppression of nonradiative recombination in the 2D/3D film. The TRPL decays and fit curves are displayed in Figure 3B, showing that the monomolecular decay time in 2D/3D perovskite was 3.50 µs against 1.85 µs in reference films under the same excitation conditions (see Supporting Information for details of the fit function). The slower TRPL decay in 2D/3D perovskite films than in control samples was related to slower nonradiative recombination and originated from the reduced density of defects in the presence of the passivating 2D layer.

We showed that the 2D layer boosts carrier lifetime due to suppressed nonradiative recombination. Here we performed space-charge limited current (SCLC) measurements to directly determine the trap density (as shown in Figure S7, Supporting Information). We fabricated an electron-only and hole-only device with FTO/TiO$_2$/perovskites/C$_{60}$/BCP/Au and FTO/PEDOT:PSS/perovskites/Spiro-OMeTAD/Au architecture, respectively. For the electron-only 2D/3D device, the trap-filled limit voltage (V_{TFL})[22] was reduced to 0.55 V compared to 0.72 eV of the pristine one. For the corresponding hole-only devices, V$_{TFL}$ decreased from 0.14 to 0.10 V with the addition of the 2D layer. These results confirmed the passivating role of the 2D layer and the resulting reduction of the density of trap states, in agreement with results obtained from PL and TRPL measurements.

We demonstrated the effect of the 2D layer on defect passivation. Now to demonstrate the impact of 2D Dion–Jacobson on

ADVANCED
SCIENCE NEWS

www.advancedsciencenews.com

**ADVANCED
MATERIALS**

www.advmat.de

holes extraction to HTL, we performed transient surface photovoltage (trSPV) excited by a 5 ns laser pulse with photon energy 1.8 eV for samples with and without the passivating 2D perovskite layer. As shown in Figure 3C, without 2D passivation, the positive signal transient increased to 206 mV within 1 µs, while the signal of 2D/3D increased to the higher value of 274 mV simultaneously. The enhanced positive SPV signal indicated that passivation by the 2D perovskite layer boosted carrier concentration. We also observe the enhanced hole extraction as a faster rise of trSPV signal in 2D/3D sample before 1 µs. The enhanced hole extraction was also confirmed in films deposited directly on glass without ETL (Figure S8, Supporting Information). Figure S9 (Supporting Information) shows the full SPV maps as a function of time and photon energy, demonstrating consistent charge extraction conditions for excitation photon energies ranging from 1.6 to 3.0 eV. From the dark J–V curves in Figure S10 (Supporting Information), it was observed that the dark current density of 2D/3D devices was an order of magnitude lower than that of the reference cells, again suggesting reduced nonradiative recombination thanks to the 2D/3D heterostructure, consistently with the SPV data.

Ultraviolet photoelectron spectroscopy (UPS) measurements were employed to determine the work function (WF) of the various stacks and band offsets at interfaces (Figure 3D). The WF of 3D and 2D films were calculated to be 4.1 and 3.9 eV, respectively. In addition, the valence band of 2D/3D perovskite was shifted down to 1.5 eV below the Fermi level, in contrast to the 1.4 eV value for pure 3D perovskite. 2D perovskite was placed at the interface with the HTL in the devices, and under illumination, it conceivably only received photoexcited electrons, not bound excitons. That is why conduction bands were well aligned; holes could be transferred to the HTL without significant energy losses. Thus, the deposition of the 2D perovskite decreased the surface WF, facilitating the transfer of holes in the 2D layer and further in HTL, as was confirmed by trSPV. The boost of carrier lifetime and charge extraction increases,[23] the solar cell's open circuit voltage (V_{oc}), consistent with recent work.[24,25] Subsequently, we demonstrated the formation mechanism of the Dion–Jacobson 2D layer on the 3D perovskite surface. Conductive atomic force microscopy (CAFM) can measure high-resolution surface morphology at microscopic scales by capturing the spatial current variations when scanning the surface. The presence of 2D perovskite organic layers on the surface caused a reduction in the electric current,[26] as confirmed by CAFM measurements shown in Figure 3E,F, where the yellow and black areas correspond to the areas with high and low conductivity, respectively. The reference sample had a uniform current throughout the surface (3.4 pA) with insulating regions corresponding to valleys between the grains in the topography image. In contrast, the 2D/3D sample showed conductivity only in some areas, providing information about the formation of the 2D layer. The 2D perovskite started growing mainly from the grain boundaries of the 3D film and then spread to the centres of the grains. The thickness of the 2D layer decreased gradually from the edge to the grain centres. The current contrast was 0.61 ± 0.06 pA for the 2D/3D perovskite and 3.2 ± 0.1 pA for pure 3D perovskite, consistent with the insulating character of the 2D perovskite. As shown in Figure S11 (Supporting Information), the AFM images indicate that the surface of 2D/3D

film had a root-mean-square (RMS) roughness close to reference.

To investigate the photovoltaic performance of 2D/3D perovskites, we fabricated reference and 2D/3D solar cells. The devices were deposited on a glass substrate with fluorine-doped tin oxide and employed a direct architecture (FTO)/TiO_2/perovskite/Spiro-OMeTAD/Au, schematically shown in **Figure 4**A. Current–voltage (J–V) characteristics of 3D and 2D/3D perovskite devices were measured under 100 mW cm^{-2} illumination (AM 1.5G), as shown in Figure 4B. The PCE of the solar cell based on 2D/3D perovskite was 19.5%, with V_{oc} = 1.197 V, J_{sc} = 20.06 mA cm^{-2} and fill factor (FF) = 81.12%. In comparison, the reference device had inferior performance, with PCE = 18.8%, V_{oc} = 1.165 V, J_{sc} = 20.38 mA cm^{-2} and FF = 79.37%. Figure 4C shows the statistics of the PCE distribution for reference and 2D/3D devices, suggesting a consistent and reproducible performance improvement thanks to the addition of the 2D layer. The corresponding statistics for V_{oc}, J_{sc}, and FF are displayed in Figure S12 (Supporting Information). Both reverse and forward scan J–V curves for reference and 2D/3D devices were measured, demonstrating minimal hysteresis, as shown in Figure S13 (Supporting Information). External quantum efficiency (EQE) spectra were also measured (Figure 4D); the integrated spectra yielded J_{sc} values of 19.85 mA cm^{-2} for the 2D/3D device and 20.12 mA cm^{-2} for the 3D device (Figure S14, Supporting Information), in good agreement with the direct measurements from the J–V curves in Figure 4B.

Using a custom-made ageing setup, we monitored the efficiency under maximum power point tracking of unencapsulated cells under 1.2 sun illumination for over 1200 h, per ISOS-L1I protocol.[27] Both tracking curves shown in Figure 4E resulted from the average of 3 PMEA and reference devices with initial PCE within the distribution reported in Figure 4C. After working for 1260 h, 2D/3D devices retained 83% of their original efficiency. The PCE of reference devices decreased to 83% of its efficiency within 180 h and degraded to 66% after 1260 h.

3. Conclusion

The 2D perovskite layer was recently broadly used to passivate the active layer in hybrid organic–inorganic PSC. We have demonstrated a strategy to improve solar cells' efficiency and intrinsic stability based on inorganic perovskite $CsPbI_3$ by depositing a Dion–Jacobson 2D phase on the 3D layer. The 2D layer employed a hydrophobic diammonium spacer and thus realized a moisture-resistant barrier, significantly slowing down the degradation of $CsPbI_3$ from the black phase to the yellow d phase in the presence of water. The 2D Dion–Jacobson layer did not represent a significant obstacle for charge transport; on the contrary, the interface between the perovskite and hole-transport layer showed reduced defects and enhanced hole extraction in the presence of the 2D layer. With this approach, the carrier lifetime of the film achieved 3.5 µs. A champion solar cell was demonstrated with PCE = 19.5% and V_{oc} = 1.197 V, which improved PCE and V_{oc} values by adding the Dion–Jacobson layer. The device retained 83% of its original efficiency after over 1200 h under 1.2 sun illumination and MPP tracking. The results presented here offer a
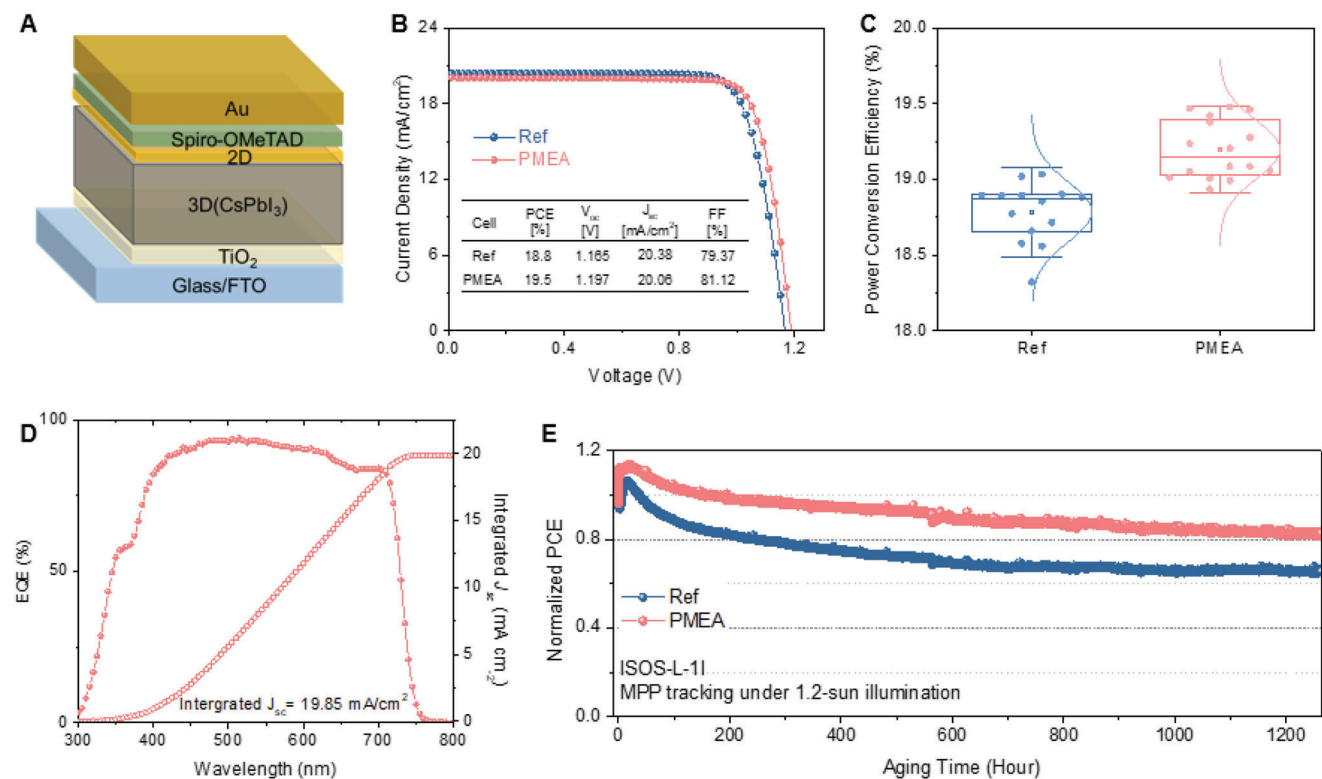
Figure 4. Photovoltaic performance of inorganic perovskite solar cells. A) Schematic device structure of the inorganic PSCs. B) J–V curves of the 3D and 2D/3D champion cells. C) Statistics of the power conversion efficiency of 3D PSCs of reference and 2D/3D PSCs. D) EQE and integrated current density of 2D/3D PSCs. E) Normalized PCEs of reference and 2D/3D PSCs of continuous MPP-tracking averaged over three devices under 1.2 sun illumination; the MPP tracking was measured through a custom-made ageing setup in an N_2 atmosphere at 25 °C.

promising path toward inorganic perovskite solar cells with sufficient operational stability and efficiency to be commercialized.

Supporting Information

Supporting Information is available from the Wiley Online Library or from the author.

Conflict of Interest

The authors declare no conflict of interest.

Data Availability Statement

The data that support the findings of this study are available from the corresponding author upon reasonable request.

[1] Y. Wang, G. Chen, D. Ouyang, X. He, C. Li, R. Ma, W.-J. Yin, W. C. H. Choy, *Adv. Mater.* **2020**, *32*, 2000186.

[2] X. Zhao, T. Liu, Q. C. Burlingame, T. Liu, R. Holley, G. Cheng, N. Yao, F. Gao, Y. L. Loo, *Science (80-.).* **2022**, *377*, 307.

[3] W. Li, M. U. Rothmann, A. Liu, Z. Wang, Y. Zhang, A. R. Pascoe, J. Lu, L. Jiang, Y. Chen, F. Huang, Y. Peng, Q. Bao, J. Etheridge, U. Bach, Y.-B. Cheng, *Adv. Energy Mater.* **2017**, *7*, 1700946.

[4] R. E. Beal, D. J. Slotcavage, T. Leijtens, A. R. Bowring, R. A. Belisle, W. H. Nguyen, G. F. Burkhard, E. T. Hoke, M. D. McGehee, *J. Phys. Chem. Lett.* **2016**, *7*, 746.

[5] W. Ahmad, J. Khan, G. Niu, J. Tang, *Sol. RRL* **2017**, *1*, 1700048.

[6] G. E. Eperon, G. M. Paternò, R. J. Sutton, A. Zampetti, A. A. Haghighirad, F. Cacialli, H. J. Snaith, *J. Mater. Chem. A* **2015**, *3*, 19688.

[7] H. Zhang, W. Xiang, X. Zuo, X. Gu, S. Zhang, Y. Du, Z. Wang, Y. Liu, H. Wu, P. Wang, Q. Cui, H. Su, Q. Tian, S. (F.) Liu, *Angew. Chem., Int. Ed.* **2023**, *62*, 202216634.

[8] Y. Wang, M. I. Dar, L. K. Ono, T. Zhang, M. Kan, Y. Li, L. Zhang, X. Wang, Y. Yang, X. Gao, Y. Qi, M. Grätzel, Y. Zhao, *Science (80-.).* **2019**, *365*, 591.

[9] X. Tan, S. Wang, Q. Zhang, H. Liu, W. Li, L. Zhu, H. Chen, *Matter* **2023**, *6*, 691.

[10] J. Yuan, D. Zhang, B. Deng, J. Du, W. C. H. Choy, J. Tian, *Adv. Funct. Mater.* **2022**, *32*, 2209070.

[11] J. He, J. Su, Z. Lin, S. Zhang, J. Ma, J. Zhang, S. Liu, J. Chang, Y. Hao, *Nano Energy* **2022**, *94*, 106960.

[12] S. M. Yoon, H. Min, J. B. Kim, G. Kim, K. S. Lee, S. I. Seok, *Joule* **2021**, *5*, 183.

[13] T. Niu, Y.-M. Xie, Q. Xue, S. Xun, Q. Yao, F. Zhen, W. Yan, H. Li, J.-L. Brédas, H.-L. Yip, Y. Cao, *Adv. Energy Mater.* **2022**, *12*, 2102973.

[14] A. H. Proppe, A. Johnston, S. Teale, A. Mahata, R. Quintero-Bermudez, E. H. Jung, L. Grater, T. Cui, T. Filleter, C.-Y. Kim, S. O. Kelley, F. De Angelis, E. H. Sargent, *Nat. Commun.* **2021**, *12*, 3472.

[15] B. Kim, S. I. Seok, *Energy Environ. Sci.* **2020**, *13*, 805.

[16] T. Liu, J. Zhang, M. Qin, X. Wu, F. Li, X. Lu, Z. Zhu, A. K.-Y. Jen, *Adv. Funct. Mater.* **2021**, *31*, 2009515.

[17] S. Tan, B. Yu, Y. Cui, F. Meng, C. Huang, Y. Li, Z. Chen, H. Wu, J. Shi, Y. Luo, D. Li, Q. Meng, *Angew. Chem., Int. Ed.* **2022**, *61*, 202201300.

[18] W. Li, X. Gu, C. Shan, X. Lai, X. W. Sun, A. K. K. Kyaw, *Nano Energy* **2022**, *91*, 106666.

[19] C. C. Stoumpos, D. H. Cao, D. J. Clark, J. Young, J. M. Rondinelli, J. I. Jang, J. T. Hupp, M. G. Kanatzidis, *Chem. Mater.* **2016**, *28*, 2852.

[20] X. Li, W. Ke, B. Traoré, P. Guo, I. Hadar, M. Kepenekian, J. Even, C. Katan, C. C. Stoumpos, R. D. Schaller, M. G. Kanatzidis, *J. Am. Chem. Soc.* **2019**, *141*, 12880.

[21] S. Ahmad, P. Fu, S. Yu, Q. Yang, X. Liu, X. Wang, X. Wang, X. Guo, C. Li, *Joule* **2019**, *3*, 794.

[22] Y. Zhong, G. Liu, Y. Su, W. Sheng, L. Gong, J. Zhang, L. Tan, Y. Chen, *Angew. Chem., Int. Ed.* **2022**, *61*, 202114588.

[23] I. Levine, A. Al-ashouri, A. Musiienko, S. Albrecht, I. Levine, A. Al-ashouri, A. Musiienko, H. Hempel, A. Magomedov, A. Drevilkauskaite, V. Getautis, D. Menzel, K. Hinrichs, T. Unold, S. Albrecht, T. Dittrich, *Joule* **2021**, *5*, 2915.

[24] L. Canil, T. Cramer, B. Fraboni, D. Ricciarelli, D. Meggiolaro, A. Singh, M. Liu, M. Rusu, C. M. Wolff, N. Phung, Q. Wang, D. Neher, T. Unold, P. Vivo, A. Gagliardi, F. De Angelis, A. Abate, *Energy Environ. Sci.* **2021**, *14*, 1429.

[25] T. Duong, H. Pham, T. C. Kho, P. Phang, K. C. Fong, D. Yan, Y. Yin, J. Peng, M. A. Mahmud, S. Gharibzadeh, B. A. Nejand, I. M. Hossain, M. R. Khan, N. Mozaffari, Y. Wu, H. Shen, J. Zheng, H. Mai, W. Liang, C. Samundsett, M. Stocks, K. McIntosh, G. G. Andersson, U. Lemmer, B. S. Richards, U. W. Paetzold, A. Ho-Ballie, Y. Liu, D. Macdonald, A. Blakers, et al., *Adv. Energy Mater.* **2020**, *10*, 1903553.

[26] C. Liang, H. Gu, Y. Xia, Z. Wang, X. Liu, J. Xia, S. Zuo, Y. Hu, X. Gao, W. Hui, L. Chao, T. Niu, M. Fang, H. Lu, H. Dong, H. Yu, S. Chen, X. Ran, L. Song, B. Li, J. Zhang, Y. Peng, G. Shao, J. Wang, Y. Chen, G. Xing, W. Huang, *Nat. Energy* **2021**, *6*, 38.

[27] M. V. Khenkin, E. A. Katz, A. Abate, G. Bardizza, J. J. Berry, C. Brabec, F. Brunetti, V. Bulović, Q. Burlingame, A. Di Carlo, R. Cheacharoen, Y.-B. Cheng, A. Colsmann, S. Cros, K. Domanski, M. Dusza, C. J. Fell, S. R. Forrest, Y. Galagan, D. Di Girolamo, M. Grätzel, A. Hagfeldt, E. von Hauff, H. Hoppe, J. Kettle, H. Köbler, M. S. Leite, S. (F.) Liu, Y.-L. Loo, J. M. Luther, et al., *Nat. Energy* **2020**, *5*, 35.

2304150 (7 of 7)